P H Y S I C A L   R E V I E W   L E T T E R S

Charge Relaxation in a Single-Electron Si/SiGe Double Quantum Dot

K. Wang,[1] C. Payette,[1] Y. Dovzhenko,[1] P. W. Deelman,[2] and J. R. Petta[1,3,*]

[1]*Department of Physics, Princeton University, Princeton, New Jersey 08544, USA*
[2]*HRL Laboratories LLC, 3011 Malibu Canyon Road, Malibu, California 90265, USA*
[3]*Princeton Institute for the Science and Technology of Materials (PRISM), Princeton University,
Princeton, New Jersey 08544, USA*
(Received 11 April 2013; published 22 July 2013)

We measure the interdot charge relaxation time T_1 of a single electron trapped in an accumulation mode Si/SiGe double quantum dot. The energy level structure of the charge qubit is determined using photon assisted tunneling, which reveals the presence of a low-lying excited state. We systematically measure T_1 as a function of detuning and interdot tunnel coupling and show that it is tunable over four orders of magnitude, with a maximum of 45 μs for our device configuration.

Semiconductor quantum dots have been widely used as probes of fundamental quantum physics and to implement charge and spin qubits [1,2]. Coherent manipulation and two-qubit entanglement have been demonstrated in GaAs double quantum dots (DQDs) and error correction techniques such as dynamic decoupling have been employed to suppress decoherence [3–6]. As an alternative host material, Si holds promise for ultracoherent spin qubits due to weak spin-orbit coupling, a centrosymmetric lattice (no piezoelectric phonon coupling), and an established route to isotopic purification [7–11]. Spin lifetimes of 6 s have been measured in Si and isotopically purified ^{28}Si crystals can support spin coherence times as long as 4 s [7,12].

While Si closely approximates a "semiconductor vacuum" for electron spins, its electronic band structure leads to potential complications that are absent in the conventional GaAs/AlGaAs two-dimensional electron gas (2DEG) system [13]. First, the ~ 3 times larger effective mass of electrons in Si requires depletion gate patterns to be scaled down significantly in order to achieve orbital level spacings comparable to those obtained in GaAs. Second, the band structure of bulk Si consists of six degenerate valleys, which introduces an additional decoherence pathway [14]. Valley degeneracy is partially lifted by uniaxial strain in a Si/SiGe heterostructure [15]. However, the energy splitting between the lowest two valleys is highly sensitive to device specifics, such as step edges in the quantum well [11,16,17]. Detailed measurements of the low-lying energy level structure, and the time scales that govern energy relaxation between these levels, are therefore needed in Si quantum dots [18].

In this Letter, we systematically measure the interdot relaxation time T_1 of a single electron trapped in a Si DQD as a function of detuning ε and interdot tunnel coupling t_c. We demonstrate a four order of magnitude variation in T_1 using a single depletion gate and obtain $T_1 = 45$ μs for weak interdot tunnel couplings [19]. We also use photon-assisted tunneling (PAT) to probe the energy level structure

of the single-electron system, demonstrating spectroscopy with an energy resolution of ~ 1 μeV. In contrast with single-electron GaAs dots, we observe low-lying excited states ~ 55 μeV above the ground state, an energy scale that is consistent with previously measured valley splittings [11,16].

Measurements are performed on an accumulation mode Si/SiGe DQD. We apply a top gate voltage $V_T = 2$ V to accumulate carriers in a Si quantum well located ~ 40 nm below the surface of the wafer [see Fig. 1(a)]. The resulting 2DEG has an electron density of $4 \times 10^{11}/\text{cm}^2$ and a mobility of $70\,000$ cm^2/V s. A 100 nm thick layer of Al$_2$O$_3$ separates the top gate from the depletion gates, which are arranged to define a DQD and a single-dot charge sensor.

We first demonstrate single-electron occupancy using radio frequency (rf) reflectometry [20]. A single quantum dot is coupled to a resonant circuit with resonance frequency $f_r = 431.8$ MHz [see Fig. 1(a)] and used as a high sensitivity charge detector [21]. The reflected amplitude A is a sensitive function of the conductance of the single-dot sensor g_Q, which is modulated by charge transitions in the DQD. We map out the DQD charge stability diagram in Fig. 1(b) by plotting the numerical derivative dA/dV_L as a function of V_L and V_R. No charging transitions are observed in the lower left corner of the charge stability diagram, indicating that the DQD has been completely emptied of free electrons. We identify this charge configuration as (0,0), where (N_L, N_R) indicates the number of electrons in the left and right dots.

The device is operated as a single-electron charge qubit near the $(1, 0) \leftrightarrow (0, 1)$ interdot charge transition. Charge dynamics are governed by the Hamiltonian $H = (\varepsilon/2)\sigma_z + t_c\sigma_x$, where σ_i are the Pauli matrices. We demonstrate tunable interdot tunnel coupling in the single-electron regime by measuring the left dot occupation $P_{(1,0)}$ as a function of detuning [see the inset of Fig. 1(b)] [1,3,22]. Qubit occupation is described by
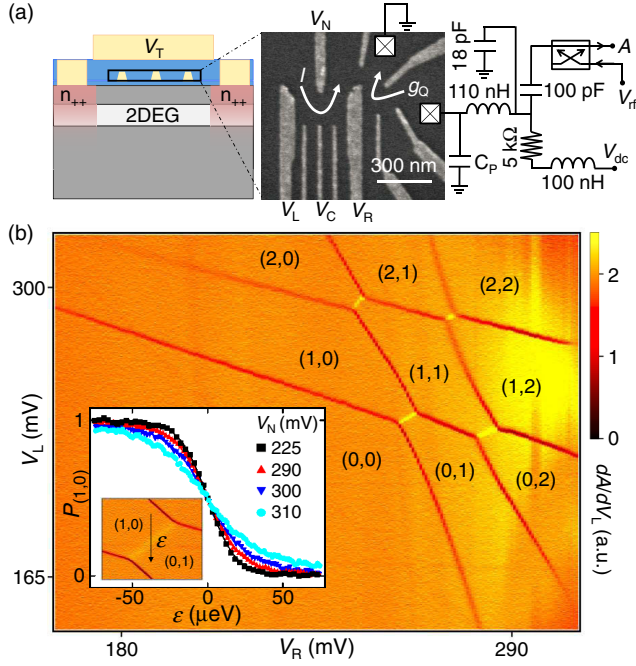
FIG. 1 (color online). (a) The DQD is operated by biasing a global top gate at voltage V_T to accumulate carriers in the quantum well (left). Local depletion gates define the DQD confinement potential (center). Charge sensing is performed using rf reflectometry (right). (b) Few electron charge stability diagram visible in the derivative of the reflected rf amplitude dA/dV_L. (N_L, N_R) indicate the number of electrons in the left and right dots. (Inset) $P_{(1,0)}$ plotted as a function of detuning, for different values of V_N, showing tunable interdot tunnel coupling at the $(1, 0) \leftrightarrow (0, 1)$ interdot charge transition.

$$P_{(1,0)} = \frac{1}{2}\left[1 - \frac{\varepsilon}{\Omega}\tanh\left(\frac{\Omega}{2k_B T_e}\right)\right], \qquad (1)$$

where k_B is Boltzmann's constant, $T_e \sim 100$ mK is the electron temperature, and $\Omega = \sqrt{\varepsilon^2 + 4t_c^2}$ is the qubit energy splitting [19,23,24]. With $V_N = 225$ mV, the interdot charge transition is thermally broadened as $2t_c < k_B T_e$. Increasing t_c by adjusting V_N leads to further broadening of the interdot transition. For $V_N = 290$, 300, and 310 mV we extract $2t_c = 3.8$, 5.9, and 9.0 GHz by fitting the data to Eq. (1). These results show that the interdot tunnel coupling can be sensitively tuned in the single-electron regime in Si.

We investigate the DQD energy level structure in Fig. 2(a), where we plot the current I as a function of V_L and V_R with a fixed source-drain bias $V_{SD} = 700$ μeV [25]. In contrast with GaAs devices, the current in the finite bias triangles is not a smooth function of gate voltage. In particular, we observe a small resonance ~ 60 μeV away from the interdot charge transition, suggesting the existence of a low-lying excited state in one of the dots. In a few electron GaAs DQD, orbital excited states are typically several meV higher in energy than the ground state [26].
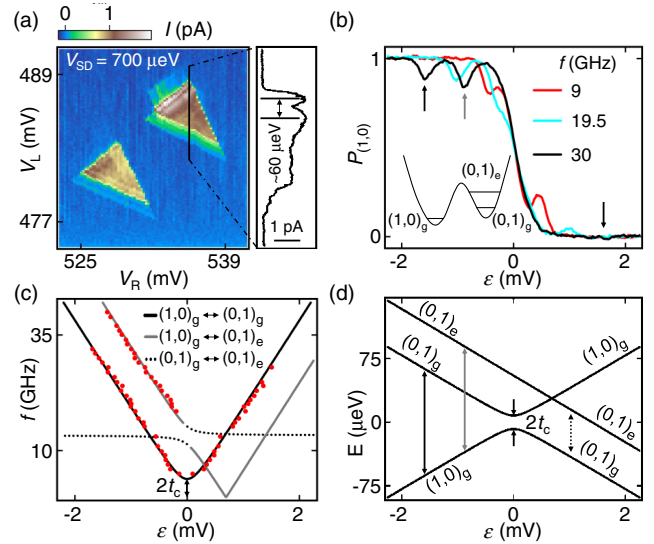

FIG. 2 (color online). (a) (left) Current I measured as a function of V_L and V_R near the $(1, 0) \leftrightarrow (0, 1)$ charge transition. A cut through the finite bias triangle (right) indicates the presence of a low-lying excited state. (b) $P_{(1,0)}$ plotted as a function of detuning ε for different excitation frequencies f. For $f \gtrsim 15$ GHz, a new PAT peak emerges (gray arrow) corresponding to the $(1, 0)_g \leftrightarrow (0, 1)_e$ transition. The appearance of this PAT peak is accompanied by the suppression of the $(1, 0)_g \leftrightarrow (0, 1)_g$ PAT peak (black arrow) at positive detuning. (c) Transition frequencies as a function of detuning and (d) energy level diagram extracted from data in (c). The data in (c) are best fit with an interdot tunnel coupling $t_c = 1.9$ GHz and an excited state energy $\Delta = 55$ μeV.

Higher energy resolution is obtained using PAT spectroscopy, in which microwaves drive charge transitions when the photon energy matches the qubit splitting $hf = \Omega$, where f is the photon frequency and h is Planck's constant. PAT transitions are directly observed as deviations from the ground state occupation in measurements of $P_{(1,0)}$ as a function of detuning [compare Fig. 2(b) and the inset of Fig. 1(b)]. For $f \lesssim 15$ GHz, the PAT peaks are symmetric around $\varepsilon = 0$ and shift to larger detuning with increasing photon energy, consistent with a simple two level interpretation [19,27]. However, for $f \gtrsim 15$ GHz, an additional PAT peak emerges at negative detuning and is not accompanied by a corresponding PAT peak at positive detuning. Figure 2(c) shows the extracted transition frequencies as a function of detuning.

The data are fit using a three level Hamiltonian that includes the left dot ground state $(1, 0)_g$, the right dot ground state $(0, 1)_g$, and a right dot excited state $(0, 1)_e$, as sketched in the inset of Fig. 2(b) (see the Supplemental Material [28]). We obtain best fit values of $t_c = 1.9$ GHz and $\Delta = 55$ μeV, consistent with the data shown in the inset of Figs. 1(b) and 2(a). Within the ~ 1 μeV resolution of our measurement, we do not observe anticrossings associated with $(0, 1)_e$. The energy eigenstates obtained from the model are plotted as a function of detuning in

Fig. 2(d). For comparison, an excited state is observed in the left quantum dot in a second device (Device 2), with $\Delta = 64 \ \mu eV$ (see the Supplemental Material [28]). For both devices, the excited state energy is highly sensitive to V_N and V_C, suggesting that it is not purely orbital in origin [17].

Several additional features observed in the data are explained by the three level model. The $(0, 1)_g \leftrightarrow (0, 1)_e$ intradot charge transition [see the dotted line in Fig. 2(c)] is not visible since the charge detector is only sensitive to interdot charge transitions. We also note that the $(0, 1)_e \leftrightarrow (1, 0)_g$ PAT peak is not visible at positive detuning. At low temperatures, the qubit population resides in the ground state $(0, 1)_g$, preventing microwave transitions from $(0, 1)_e$ to $(1, 0)_g$. Finally, the $(0, 1)_g \leftrightarrow (1, 0)_g$ PAT peak is suppressed when $\varepsilon > \Delta$ due to population trapping in $(0, 1)_e$.

We measure the interdot charge relaxation time T_1 by applying microwaves to V_L with a 50% duty cycle and varying the pulse period τ [see Fig. 3(a)]. We focus on the $(1, 0)_g \leftrightarrow (0, 1)_g$ transition at negative detuning, where the high energy state $(0, 1)_e$ is not populated. Simulations of $P_{(1,0)}$ as a function of time t for $\tau = 1 \ \mu s$ are shown in Fig. 3(a) for three realistic values of T_1. During the first half of the pulse cycle, microwaves drive the $(1, 0)_g \leftrightarrow (0, 1)_g$ charge transition, resulting in an average $P_{(1,0)} = 0.5$. The microwave excitation is then turned off, leading to charge relaxation during the second half of the pulse cycle, with $P_{(1,0)}$ approaching 1 on a time scale set by T_1.

In the inset of Fig. 3(b), we plot $P_{(1,0)}$ as a function of detuning for $\tau = 10$ ns and $\tau = 100 \ \mu s$. As expected, the PAT peak is smaller for longer periods due to charge relaxation. Specifically, in the limit $\tau \ll T_1$, there is not sufficient time for relaxation to occur during the second half of the pulse cycle, leading to a time averaged value of $P_{(1,0)} = 0.5$. In contrast, in the limit $\tau \gg T_1$, relaxation happens quickly, leaving $P_{(1,0)} = 1$ for the majority of the second half of the pulse cycle. Due to experimental limitations, such as frequency dependent attenuation in the coax lines and finite pulse rise times at small τ, we are unable to drive the transitions to saturation for some device configurations. To extract T_1 we therefore fit the raw $P_{(1,0)}$ data as a function of τ to the form

$$P_{(1,0)} = P_{max} + (P_{min} - P_{max}) \frac{2T_1(1 - e^{-\tau/(2T_1)})}{\tau}, \quad (2)$$

where P_{max} and P_{min} account for the limited visibility of the PAT peaks (see Ref. [19] and the Supplemental Material [28]). Extracted T_1 values are insensitive to the rescaling of the data via P_{max} and P_{min}.

The interdot charge relaxation rate is strongly dependent on the interdot tunnel coupling. This variation is directly visible in the data shown in Fig. 3(b) for $V_N = 225, 250,$ and 265 mV. To facilitate a direct comparison of the data, we plot the normalized electron occupation $P^*_{(1,0)} = 0.5 + 0.25 (P_{(1,0)} - P_{min})/(P_{max} - P_{min})$, using the values of P_{min} and P_{max} extracted from fits to Eq. (2) (see the Supplemental Material [28]). In Fig. 3(c), we plot T_1 over a wide range of V_N for two different excitation frequencies. We see a longer characteristic relaxation time for larger interdot barrier heights, with a maximum observed value of 45 μs. The same overall trend is observed in data from Device 2 [see Fig. 3(d)] where the interdot tunnel coupling was tuned using V_C. Interdot tunnel coupling is only measurable in charge sensing when $2t_c > k_B T_e$ [23]. For Device 1 [see Fig. 3(c)] we obtain $2t_c = 2.4, 3.8,$ and 5.9 GHz for $V_N = 280, 290,$ and 300 mV and for Device 2 [see Fig. 3(d)] we obtain $2t_c = 3.2$ GHz for $V_C = -325$ mV.

The detuning dependence of T_1 is investigated in Fig. 4(a), where we plot T_1 as a function of $f \propto \Omega$ for the $(0, 1)_g \leftrightarrow (1, 0)_g$ transition [3,22]. Data are taken at $f = 12.3, 19.5, 25.9,$ and 30.0 GHz, as indicated by the arrows in the energy level diagram in the upper panel of Fig. 4(a). Our data indicate that T_1 increases weakly as a function of detuning for the range of frequencies accessible in our cryostat.

To further investigate the excited state, we measure T_1 for the $(0, 1)_g \rightarrow (1, 0)_g$ and the $(0, 1)_e \rightarrow (1, 0)_g$ relaxation processes at the same values of f [see the bottom panel of Fig. 4(b)]. In contrast with the $(0, 1)_g \rightarrow (1, 0)_g$ relaxation process, $(0, 1)_e$ can relax via two distinct pathways [see the top panel of Fig. 4(b)]. The first relaxation process is a direct transition from $(0, 1)_e \rightarrow (1, 0)_g$ with a rate Γ_e, while
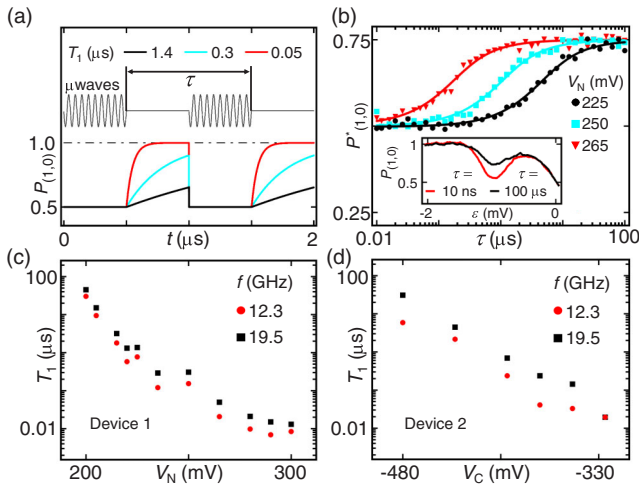

FIG. 3 (color online). (a) Pulse sequence used to measure T_1 and simulated qubit response. $P_{(1,0)} = 0.5$ when resonant microwaves drive transitions between $(0, 1)_g$ and $(1, 0)_g$, and approaches 1 on a time scale set by T_1 when the microwaves are turned off. (b) $P^*_{(1,0)}$ as a function of τ extracted for different V_N at $f = 19.5$ GHz. Fits to the data give $T_1 = 1.4, 0.3,$ and 0.05 μs for $V_N = 225, 250,$ and 265 mV. (Inset) Comparison of typical PAT peaks at different τ, with fixed $V_N = 225$ mV and $f = 25.9$ GHz. (c) T_1 as a function of V_N in Device 1. (d) T_1 as a function of V_C in Device 2.
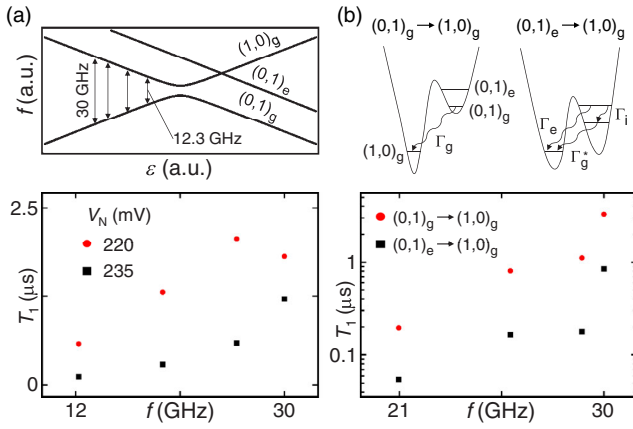
FIG. 4 (color online). (a) T_1 increases weakly with f for the $(0, 1)_g \rightarrow (1, 0)_g$ transition. (b) T_1 for the $(0, 1)_g \rightarrow (1, 0)_g$ and $(0, 1)_e \rightarrow (1, 0)_g$ transitions as a function of f with $V_N = 250$ mV (lower). There are two $(0, 1)_e \rightarrow (1, 0)_g$ relaxation pathways (upper).

the second pathway proceeds via intradot charge relaxation to $(0, 1)_g$ with a rate Γ_i followed by an interdot transition to $(1, 0)_g$ with a rate Γ_g^*. We find that the $(0, 1)_e \rightarrow (1, 0)_g$ relaxation is faster than the $(0, 1)_g \rightarrow (1, 0)_g$ relaxation for the same energy splitting.

The shorter excited state lifetime is consistent with either a fast direct relaxation rate Γ_e or a fast intradot relaxation followed by an interdot transition. Neglecting valley physics, one would expect $\Gamma_e > \Gamma_g$ due to the more extended excited state orbital wave function. Considering valley physics, and assuming that direct interdot charge relaxation is limited by the intervalley relaxation rate, then $\Gamma_e < \Gamma_g$. The role of valley states is somewhat debated and the nature of the right dot excited state is unclear [18]. Therefore, to obtain a rough estimate of Γ_i, we assume $\Gamma_g = \Gamma_e$ (since the level detuning is the same). Taking the measured excited state $T_1 = 55$ ns at $f = 21.0$ GHz, we obtain a lower bound estimate of $\Gamma_i \sim 1.5 \times 10^7$ s^{-1} [29].

We modify the results of Raith *et al.* to allow the calculation of phonon mediated charge relaxation rates considering only intravalley relaxation in the far detuned limit ($|\varepsilon| \gg t_c$), assuming Gaussian wave functions for the nonhybridized charge states, with dot radius a and dot separation $2d$ (see the Supplemental Material [28] and Ref. [30]). The electron-phonon coupling Hamiltonian in a Si quantum well takes the form

$$H_{\text{e-ph}} = i \sum_{\mathbf{Q}, \lambda} \left(\frac{\hbar |\mathbf{Q}|}{2\rho V c_\lambda} \right)^{1/2} D_{\mathbf{Q}}^\lambda (a_{\mathbf{Q}, \lambda}^\dagger e^{i\mathbf{Q} \cdot \mathbf{r}} - a_{\mathbf{Q}, \lambda} e^{-i\mathbf{Q} \cdot \mathbf{r}}), \tag{3}$$

where

$$D_{\mathbf{Q}}^\lambda = (\Xi_d \hat{\mathbf{e}}_{\mathbf{Q}}^\lambda \cdot \hat{\mathbf{Q}} + \Xi_u \hat{e}_{\mathbf{Q},z}^\lambda \hat{Q}_z). \tag{4}$$

Here $a_{\mathbf{Q}, \lambda}$ ($a_{\mathbf{Q}, \lambda}^\dagger$) is the annihilation (creation) operator for phonons belonging to branch λ ($\lambda = $ TA1, TA2 for transverse phonons and $\lambda = $ LA for longitudinal phonons) with wave vector $\mathbf{Q}$, and speed of sound in Si c_λ. V is the volume of the Si quantum well layer and ρ is the density of Si. Ξ_u and Ξ_d are the shear and dilation deformation potential constants, and $\hat{\mathbf{e}}_{\mathbf{Q}}^\lambda$ and $\hat{\mathbf{Q}}$ are the phonon unit polarization vector and the phonon unit wave vector [30]. Using realistic parameters, T_1 values calculated in this model are in order of magnitude agreement with our data (see the Supplemental Material [28]). However, the predictions are exponentially sensitive to a and d, quantities that are difficult to accurately determine. Moreover, the model predicts a relaxation rate that increases with energy splitting for the range of detunings accessed in our experiment, following the power law $\Gamma_1 = 1/T_1 \propto \Omega^3$, whereas we observe a rate that decreases weakly with increasing detuning (see the Supplemental Material [28]). This discrepancy may be due to a detuning dependent t_c or contributions from other relaxation channels, such as charge noise [31].

In summary, we have measured charge relaxation times in a single-electron Si/SiGe DQD, demonstrating a four order of magnitude variation of T_1 with gate voltage. Energy level spectroscopy indicates the presence of a low-lying excited state. From the estimated dot radius $a \sim 38$ nm, we expect orbital level spacings on the order of 1 meV, a factor of 18 larger than the value obtained from PAT spectroscopy ($\Delta = 55$ μeV) [32]. This suggests that the low-lying excited state is a valley-orbit mixed state [33].

*petta@princeton.edu

[1] D. Loss and D. P. DiVincenzo, Phys. Rev. A **57**, 120 (1998).
[2] R. Hanson, L. P. Kouwenhoven, J. R. Petta, S. Tarucha, and L. M. K. Vandersypen, Rev. Mod. Phys. **79**, 1217 (2007).
[3] J. R. Petta, A. C. Johnson, J. M. Taylor, E. A. Laird, A. Yacoby, M. D. Lukin, C. M. Marcus, M. P. Hanson, and A. C. Gossard, Science **309**, 2180 (2005).

[4] J. M. Taylor, J. R. Petta, A. C. Johnson, A. Yacoby, C. M. Marcus, and M. D. Lukin, Phys. Rev. B **76**, 035315 (2007).

[5] H. Bluhm, S. Foletti, I. Neder, M. Rudner, D. Mahalu, V. Umansky, and A. Yacoby, Nat. Phys. **7**, 109 (2011).

[6] M. D. Shulman, O. E. Dial, S. P. Harvey, H. Bluhm, V. Umansky, and A. Yacoby, Science **336**, 202 (2012).

[7] A. Morello et al., Nature (London) **467**, 687 (2010).

[8] M. Xiao, M. G. House, and H. W. Jiang, Phys. Rev. Lett. **104**, 096801 (2010).

[9] C. B. Simmons et al., Phys. Rev. Lett. **106**, 156804 (2011).

[10] J. R. Prance et al., Phys. Rev. Lett. **108**, 046808 (2012).

[11] B. M. Maune et al., Nature (London) **481**, 344 (2012).

[12] A. M. Tyryshkin et al., Nat. Mater. **11**, 143 (2012).

[13] D. D. Awschalom, L. C. Bassett, A. S. Dzurak, E. L. Hu, and J. R. Petta, Science **339**, 1174 (2013).

[14] T. Ando, A. B. Fowler, and F. Stern, Rev. Mod. Phys. **54**, 437 (1982).

[15] F. Schäffler, Semicond. Sci. Technol. **12**, 1515 (1997).

[16] S. Goswami et al., Nat. Phys. **3**, 41 (2007).

[17] M. Friesen and S. N. Coppersmith, Phys. Rev. B **81**, 115324 (2010).

[18] C. Tahan and R. Joynt, arXiv:1301.0260.

[19] J. R. Petta, A. C. Johnson, C. M. Marcus, M. P. Hanson, and A. C. Gossard, Phys. Rev. Lett. **93**, 186802 (2004).

[20] R. J. Schoelkopf, P. Wahlgren, A. A. Kozhevnikov, P. Delsing, and D. E. Prober, Science **280**, 1238 (1998).

[21] C. Barthel, M. Kjærgaard, J. Medford, M. Stopa, C. M. Marcus, M. P. Hanson, and A. C. Gossard, Phys. Rev. B **81**, 161308 (2010).

[22] Y. Nakamura, Yu. A. Pashkin, and J. S. Tsai, Nature (London) **398**, 786 (1999).

[23] L. DiCarlo, H. J. Lynch, A. C. Johnson, L. I. Childress, K. Crockett, C. M. Marcus, M. P. Hanson, and A. C. Gossard, Phys. Rev. Lett. **92**, 226801 (2004).

[24] C. B. Simmons et al., Nano Lett. **9**, 3234 (2009).

[25] W. G. van der Wiel, S. De Franceschi, J. M. Elzerman, T. Fujisawa, S. Tarucha, and L. P. Kouwenhoven, Rev. Mod. Phys. **75**, 1 (2002).

[26] A. C. Johnson, C. M. Marcus, M. P. Hanson, and A. C. Gossard, Phys. Rev. B **71**, 115333 (2005).

[27] C. H. van der Wal, A. C. J. ter Haar, F. K. Wilhelm, R. N. Schouten, C. J. P. M. Harmans, T. P. Orlando, S. Lloyd, and J. E. Mooij, Science **290**, 773 (2000).

[28] See Supplemental Material at http://link.aps.org/supplemental/10.1103/PhysRevLett.111.046801 for data from a second device and a more detailed description of the theoretical model, measurement techniques, and data analysis.

[29] T. Fujisawa, D. G. Austing, Y. Tokura, Y. Hirayama, and S. Tarucha, Nature (London) **419**, 278 (2002).

[30] M. Raith, P. Stano, and J. Fabian, Phys. Rev. B **86**, 205321 (2012).

[31] O. Astafiev, Y. A. Pashkin, Y. Nakamura, T. Yamamoto, and J. S. Tsai, Phys. Rev. Lett. **93**, 267007 (2004).

[32] L. P. Kouwenhoven, C. M. Marcus, P. L. McEuen, S. Tarucha, R. M. Westervelt, and N. S. Wingreen, in *Mesoscopic Electron Transport, Proceedings of the NATO Advanced Studies Institute, Series E*, Vol. 345, edited by L. L. Sohn, L. P. Kouwenhoven, and G. Schon (Kluwer Academic, Dordrecht, 1997).

[33] C. H. Yang, A. Rossi, R. Ruskov, N. S. Lai, F. A. Mohiyaddin, S. Lee, C. Tahan, G. Klimeck, A. Morello, and A. S. Dzurak, arXiv:1302.0983.